Journal of the Brazilian Society of Mechanical Sciences and Engineering (2023) 45:13
https://doi.org/10.1007/s40430-022-03941-w

TECHNICAL PAPER

Topology optimization of cylindrical shells with cutouts for maximum buckling strength

Yusuf Gokyer[1] · **Fazil O. Sonmez**[1]

Received: 22 August 2022 / Accepted: 30 November 2022

Abstract
In the presence of cutouts, the buckling strength of shell structures under compression significantly decreases. In order to compensate this, these structures are reinforced with stiffeners. In this study, the objective is to optimize the stiffener geometry and pattern on a cylindrical shell with two square holes to maximize the buckling load capacity without increase in its weight. A finite element model is developed to evaluate the buckling load of the structure. A good correlation is observed between the nonlinear analysis results of the model and the numerical and experimental results reported in the literature. Optimization is achieved in two levels. In the first level, topology optimization is performed to obtain the optimal stiffener pattern over the shell surface based on linear eigenvalue buckling analysis. In the second level, the stiffener heights and the shell thickness are optimized using a local search algorithm, Nelder–Mead; the buckling load levels are obtained by carrying out nonlinear buckling analyses in ANSYS. A Python code is developed to implement the optimization method and conduct analyses in ANSYS. The results show that stiffeners need to be introduced around the cutouts and the regions near the top and bottom edges for maximum buckling load capacity. The results also reveal that stiffeners on the mid lateral surfaces of the cylinder do not make significant contribution to the buckling strength. The bucking load of the optimized stiffened geometry is 22% higher than that of the unreinforced geometry having the same weight.

Keywords Stiffened cylindrical shells · Metals · Axial load · Buckling · Structural optimization · FEA

1 Introduction

Stiffeners are secondary structural parts attached to main structure in order to make it stiffer, or more resistant to deformation, under bending loads. Increasing wall thickness is a well-known approach to improve the flexural stiffness and strength, but the same stiffness and strength can be obtained by using stiffeners with much less use of material. Stiffeners are commonly used to provide extra rigidity in such systems where weight plays a critical role such as rocket launch systems, aircraft engines, and aircrafts. Apart from stiffening the whole structure, sometimes stiffeners are only used for locally increasing rigidity especially around cutouts that may significantly decrease the buckling strength of the structure. For example, wind turbine towers have a considerably large hole used as entrance and stiffeners need to be used to recover the loss in the load-carrying capacity of the structure due to the cutout. In weight-critical applications, the topology and size of the stiffeners should be judiciously chosen to make the best use of material. For this purpose, a systematic methodology should be adopted to find the optimum stiffener configuration.

1.1 Literature review

A number of researchers [1–24] studied the buckling behavior of stiffened cylindrical shells made of metals. Some of them [1–17] investigated the influence of stiffener geometry on the buckling strength of cylindrical shells made of steel or aluminum with no cutouts under axial compressive loading. Some optimized [7–17] the design of the stiffeners on the shell surface. Weller and Singer [1] experimentally studied the effect of stiffeners on the buckling behavior. Cylinders stiffened by stringers having different cross sections and different spacing were tested. All stiffened shells

Technical Editor: João Marciano Laredo dos Reis.

✉ Fazil O. Sonmez
sonmezfa@boun.edu.tr

[1] Department of Mechanical Engineering, Bogazici University, Bebek, 34342 Istanbul, Turkey

Published online: 12 December 2022

provided larger buckling resistance compared to equal-weight uniform shells. Hotala and Skotny [2] experimentally and numerically investigated buckling strength of steel silos having stiffeners with different shapes and lengths. The results showed that use of short ribs interconnected with a circumferential ring highly decreased meridional stresses and increased load-carrying capacity of such structures. Huishen et al. [3] conducted a theoretical study on the buckling and post-buckling behavior of stiffened shells based on the boundary layer theory. Zhu et al. [5] presented a new design for a ring-type stiffened shell with a combination of large and small rings having T and L-shaped cross sections. By optimizing the height of the stiffeners and the span of T-shaped stiffener rings, the buckling load-carrying capacity was maximized. Foryś [7] optimized the internal diameter and the number of rings of ring-stiffened shells to maximize the critical buckling load by using modified particle swarm optimization method. Constraints were imposed on the volume of the material and the stability of the post-buckling behavior. Bagheri et al. [8] also obtained optimum design of a ring-stiffened shell using genetic algorithm (GA). The design variables were shell thickness, number of stiffeners, stiffener dimensions, and spacing between the stiffeners. The results showed that the optimized design had lower structural weight, higher natural frequency, and higher buckling load-carrying capacity. Sadeghifara et al. [9] conducted a multi-objective optimization of a cylindrical shell stiffened by orthogonal grids (stiffeners in the axial and circumferential directions) to maximize the buckling load and minimize the weight. Optimization was performed by varying thickness, width, and number of stiffeners, and spacing for rectangular, C, I, and hat-shaped stiffener sections. The I-section and the rectangular section proved to be the most and least effective geometry on the buckling strength, respectively. Wang et al. [11] maximized the load-carrying capacity of cylindrical shells stiffened with different grid patterns by varying the shell thickness and the heights and number of axial and circumferential stiffeners. They considered four different types of hierarchical stiffener patterns, which included major and minor stiffeners having different dimensions. Zhao et al. [13] and Tian et al. [14], similarly, considered a hierarchical grid pattern having a primary grid and a secondary grid with a smaller cell size. The design variables were chosen as the width and height of the primary and secondary group of stiffeners and their numbers.

Cutouts significantly reduce the buckling strength of cylindrical shells [22, 23]. Reduction in strength significantly depends on the size of the cutout. Starnes [24] found that the buckling load of a cylinder with a circular hole depended on a parameter proportional to the hole radius divided by the square root of the product of the shell radius and thickness. Detrimental effects of cutouts can be offset by making use of stiffeners. Several researchers [18–21] investigated the effects of stiffeners on the buckling behavior of cylinders having cutouts and some of them [20, 21] optimized their geometry. Grazijahani et al. [18] studied the buckling behavior of cylinders with a cutout similar in form to wind turbine entrance doors. Steel tubes with rectangular, elliptical, and oval-shaped cutouts of different sizes at different positions on the shell surface were tested to determine their effects on the load-carrying capacity. Then, two stringers with rectangular cross section were welded close to the rectangular cutout. It was found that the stiffened shell had buckling load-carrying capacity %33 higher than that of the unstiffened cylinder. Alsalah et al. [19] numerically investigated various stiffener configurations around cutouts and tried to recover buckling load-carrying capacity lost due to the opening. They considered cylindrical shells made of steel with rectangular cutouts and determined the influence of the shell thickness, cutout dimensions, and location on buckling load. The results showed that the cutout shape had minimal influence on the buckling load, whereas the size had much more influence. Besides, it was found that the frame ring configuration, where stiffeners were placed all around the cutout, could fully recover the lost capacity. Hao et al. [20] minimized the weight of an aluminum cylindrical shell with rectangular and circular cutouts using a genetic algorithm. They subdivided the structure into panels and used a different stiffener pattern on the panels with a cutout. The design variables were the dimensions of the stiffeners, the shell thickness, and the number of stiffeners for each sub-panel with a constraint on the collapse load. In a similar study, Hao et al. [21] considered an aluminum cylindrical shell in a launch vehicle with multiple cutouts. They used curvilinear stiffeners around the cutouts and straight ones away from them. The objective of the optimization was to increase the collapse buckling load with a constraint on the mass. The design variables were the number of the axial and circumferential curvilinear stiffeners, shell thickness, stiffener dimensions, and the parameters defining the positions of the curvilinear stiffeners. Tian et al. [25] minimized the weight of curved shells having complex shapes by optimizing the main shell thickness, the dimensions, and the number of stiffeners. Li et al. [26] applied a similar method to optimize a thin-walled pressure vessel with variable thickness.

In early studies [7–14], researchers were mainly interested in the optimization of stiffener dimensions such as height and width and the stiffeners were applied uniformly over the entire shell surface. Some studies [8, 9, 11, 13, 14, 26] also optimized the number of stiffeners and spacing between them, but the stiffener patterns were the same. Besides, only few studies [18–21] considered geometrical imperfections like cutouts on shell surface and conducted optimization. In recent years, hybrid stiffener models with varying stiffener dimensions have gained importance [17, 20, 21], because more weight reduction is thus possible, but

the same stiffener pattern was applied either on the entire surface or the sub-panels of the shell structures. In the previous studies, the pattern of the stiffeners was predetermined. In the present study, on the other hand, not only the stiffener dimensions, but also the stiffener pattern on the entire lateral surface is optimized.

It is worth pointing out that due to limitations of the convectional manufacturing techniques and weldability, it was not possible to produce such complex stiffener patterns on shell surfaces in the past. Now, with the help of the latest manufacturing technologies such as 3D printers, it is possible to produce complex metal structures; thus, any stiffener configuration is feasible for weight reduction and better structural performance especially for the aviation industry.

It should be noted that there were a great number of studies aimed to increase buckling resistance of stiffened cylindrical composite panels by optimizing stiffener cross section, pattern, ply angle, material properties, panel thickness, etc. However, because only metal cylindrical shell structures are considered in this study, the literature on the optimization of stiffened composite structures is not discussed.

1.2 Problem statement and objective

In this study, a thin-walled metal cylinder containing two holes is considered as shown in Fig. 1. The cylinder is subjected to an axial compressive force. For this reason, it is liable to buckling failure. It is well known that holes may cause significant decrease in the buckling strength of structures. Increasing thickness is not an effective way of improving the buckling strength in weight-critical applications compared to the use of stiffeners. For these reasons, the goal of this study is to find the optimum layout of the stiffeners that maximizes the buckling strength of the cylindrical shell structure with cutouts. The stiffeners in this study are not modeled as separate structural parts added to the main cylindrical shell structure, but as integral parts of the main shell with locally increased shell thickness. In this way, the optimization problem is posed as finding the optimum thickness distribution of a 2D structure, i.e., topology optimization, in other words topography optimization. First, a finite element model of the structure and loading is developed and it is validated using the experimental results of the bucking test of a similar structure reported in a previous study. The optimization is achieved in two levels. First, topology of the stiffeners is optimized. In this way, the optimum stiffener layout, in other words the thickness distribution of the shell structure is determined. In the second level, using the stiffener pattern determined in the first level, heights of the stiffeners and the main shell thickness are optimized.

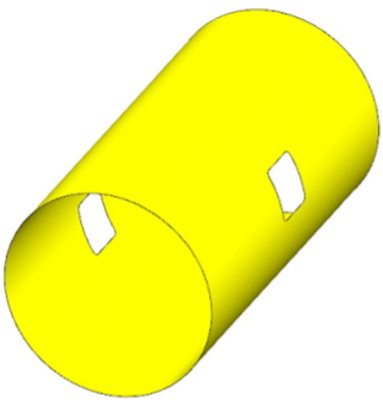

Fig. 1 The reference geometry for optimization

2 Methodology

First, a finite element (FE) model is developed to study the structural behavior of stiffened cylinders with cutouts under axial compressive loading. In order to validate the FE model, its predictions are compared with the numerical and experimental results reported by Han et al. [23] for thin-walled cylinders with cutout under uniform axial compressive loading. Comparisons are made for two different cylinders having length/diameter ratio equal to $L/D = 2$ and 5. Mesh sensitivity study is performed with various mesh sizes to find a suitable mesh size that gives results with reasonably small amount of error without long computational times. The meshed model is exported to ANSYS, which is used as solver for linear and nonlinear buckling analyses. The resulting load vs. end-shortening curves are compared with the numerical and experimental results reported in the reference study.

After validating the nonlinear FE model, a thin-walled cylindrical shell with dimensions similar to the ones in the reference study [23] is considered in this study for optimization. Its mass is taken as the reference value, because it is desired to increase the load-carrying capacity by using stiffeners using the same amount of mass as the unstiffened reference shell. Optimization is achieved in two levels. In the first level, the model is run in OptiStruct using linear buckling analysis and the optimum topology is obtained. Linear buckling analysis is preferred in the first level because of its computational efficiency. Three different stiffener patterns are identified based on the results of the topology optimization. In the second level of the optimization, the heights of the stiffeners are optimized using a local search algorithm, Nelder–Mead, to maximize the load-carrying capacity without increasing the mass. Nelder–Mead is preferred, because it is a zero-order search algorithm, which does not require derivatives of the objective function, and it is quite stable. The buckling load of the configurations generated by the search algorithm during optimization is determined by

conducting nonlinear finite element analysis. A Python code is written to integrate Nelder–Mead with ANSYS. It generates ANSYS Parametric Design Language (APDL) code that updates the FE model and carries out a nonlinear analysis for each configuration generated by Nelder–Mead algorithm in each iteration. Based on the critical buckling load calculated by ANSYS, the search algorithm determines the next configuration. Depending on the values of the stiffener thickness provided by the algorithm, Python code calculates the shell thickness such that the mass remains the same as the mass of the unstiffened shell. The methodology is explained in detail in the following sections.

3 FE model and its validation

3.1 Geometry and material

Three different shell geometries in the reference study [23] are considered to validate the FE model. The cylinders have two different thicknesses, which are 0.889 and 0.0889 mm. The diameter of all the cylinders is 40 mm. The length of the relatively thick cylinder is 200 mm. The thinner cylinders have two different lengths, 80 mm and 200 mm. The cylinders have a square cutout with dimensions 7.5 mm × 7.5 mm located at the middle as seen in Fig. 2. The radius of curvature of the fillets at the corners of the hole is 1.00 mm, which are introduced to reduce stress concentration. Geometrical dimensions of the analyzed cylinders shown in Fig. 2 are given in Table 1.

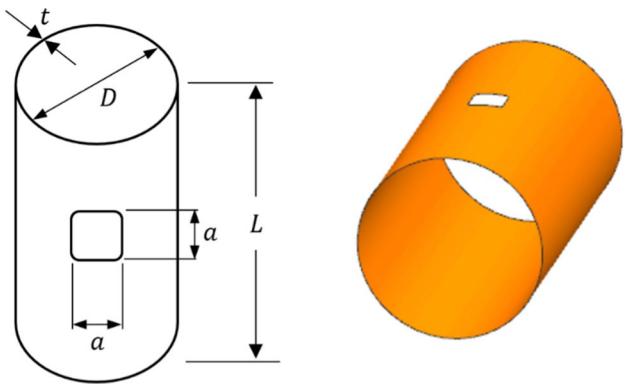

Fig. 2 The cylindrical shell geometry used to validate the FE model

The material of the cylinders is AL 6061-T6 alloy. The stress–strain curve of the material reported by the reference study [23] is used in the FE model. The elastic modulus and Poisson's ratio of the material are 68.95 GPa and 0.33, respectively. Its yield strength is 276 MPa. Multi-linear isotropic hardening material model is used for the nonlinear analyses in ANSYS. In isotropic hardening, the yield surface expands uniformly during plastic flow. This is well suited for simulating large-strain deformations. In linear buckling analyses, on the other hand, only elastic modulus and Poisson's ratio are used as material property.

3.2 Element type and boundary conditions

Shell-181 element is used to mesh the cylindrical area, which is very suitable for analyzing thin to moderately thick shell structures undergoing linear or large-strain nonlinear deformations [27]. It is a four-node element with six degrees of freedom at each node; translations in the x, y, and z directions, and rotations about the x, y, and z axes. The element formulations are based on the first-order (Mindlin-Reissner) shear deformation theory. The number of integration points through the thickness is five. The mesh around the hole is refined. The finite element mesh is shown in Fig. 3.

The boundary conditions in the finite element model are specified to simulate the loading conditions in the experiments of the reference study [23], where the ends of the cylinders were held by rigid steel sleeves as shown in Fig. 5 and the cylinders were pressed from the top. Accordingly, as boundary condition, the axial force is distributed to the nodes on the top around the circumference of the cylindrical shell. It is coupled with the constraint of uniform displacement in the z (axial) direction. Vertical displacement is restrained at the bottom edge and left free at the top end, while lateral displacements in x and y directions are prevented at both ends. Rotational degrees of freedom in all directions are restrained at the bottom and top ends.

3.3 Linear (eigenvalue) and nonlinear (collapse) analyses

A linear FE buckling analysis is performed to predict the theoretical critical buckling load (the first eigenvalue) of the shell structure. The eigenvalue analysis uses an iterative algorithm that yields the eigenvalue and the mode shape. The eigenvalue,

Table 1 Dimensions of the analyzed shell geometries depicted in Fig. 2

	D (mm)	L (mm)	t (mm)	L/D	D/t	a (mm)
Geometry 1	40	200	0.889	5	45	7.5
Geometry 2	40	80	0.0889	2	450	7.5
Geometry 3	40	200	0.0889	5	450	7.5

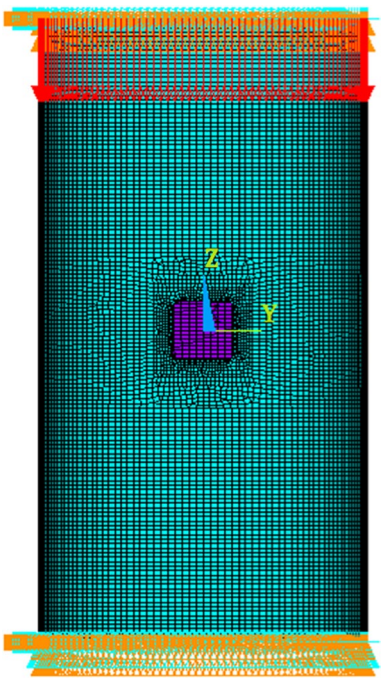

Fig. 3 The FE model with the boundary conditions. The global mesh size is about 1.0 mm

λ_i, (load factor) represents the ratio between the critical buckling load, p_{cr}, and the initially applied load, N_i, as follows:

$$\lambda_i = \frac{p_{cr}}{N_i} \tag{1}$$

Accordingly, the critical buckling load, p_{cr}, is obtained by multiplying the axially applied force on the structure, N_i, with the eigenvalue, λ_i, calculated by the FE analysis.

The geometrical imperfection due to the cutout leads to nonlinearities, which cannot be accounted for by the eigenvalue analysis. However, linear buckling analysis should be considered as a first approximation. It is necessary to conduct a nonlinear analysis to accurately predict the unstable mechanical response of the cylindrical shell with cutout. The basic form of the eigenvalue buckling analysis can be expressed [28] as follows:

$$[K_e]\{\phi_i\} = \lambda_i[K_\sigma]\{\phi_i\} \tag{2}$$

where $[K_e]$ is the elastic stiffness matrix, $\{\phi_i\}$ is the eigenvector indicating the mode shape, λ_i is the eigenvalue indicating the load factor, and $[K_\sigma]$ is the initial stress matrix. In the nonlinear analysis, the option in the FEA software for large deflections is turned on. A gradually increasing load is applied to find the load level at which the structure becomes unstable. The nonlinear analysis takes into consideration both geometric and material nonlinearities. Change in the shell thickness during loading is also taken into account. Nonlinear analyses for each of the three geometries are conducted using the arc-length method as in the reference study [23] to obtain the post-buckling behavior.

3.4 Convergence study for mesh sizing

In order to determine an appropriate mesh size, geometry 2 is chosen and several linear and nonlinear buckling analyses are conducted with different mesh sizes. The results are given in Table 2 and Fig. 4. Considering the convergence of the solution in terms of buckling load, 0.5 mm mesh size is used in both linear and nonlinear analyses, which results in 98,000 elements. The refined mesh size around the hole is about one sixth of the global mesh size.

There is significant difference between the results of the linear and nonlinear buckling analyses because of the geometric nonlinearity introduced by the hole. Linear eigenvalue buckling analysis cannot accurately predict the effect of geometric nonlinearity. In the reference study [23], the cylinder was analyzed for different hole sizes. If there was no hole, the linear buckling analysis yielded a buckling load that was 5.1% higher

Table 2 The values of the critical buckling load evaluated by the linear and nonlinear buckling analyses for different mesh sizes

	Average mesh size (mm)	Critical buckling load (N)
Linear analysis	3	494.1
	2	371.5
	1	336.4
	0.875	331.1
	0.675	328.1
	0.500	328.3
	0.375	328.3
Nonlinear analysis	0.675	732.9
	0.500	734.7
	0.375	735.2

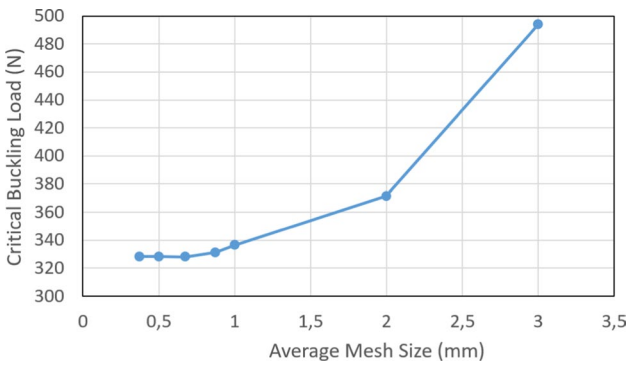

Fig. 4 Convergence of the critical buckling load to 328.3 N with smaller mesh size

than that of the nonlinear analysis. If the size of the cutout was 5.3×5.3 mm, the linear analysis gave 25.2% lower value. With 7.5×7.5 mm hole, 41.0% lower value was obtained. With 10.6×10.6 mm hole, 55.3% lower value was obtained, the same as in Table 2. The larger the hole, the larger the effect of the geometric nonlinearity, and the larger the difference between the results of the linear and nonlinear analyses.

3.5 Validation of the finite element model

Linear and nonlinear buckling analyses are carried out for the three geometries. The resulting load vs. end-shortening curve for relatively thick shell is compared with the numerical and experimental results in the reference study [23]. The critical buckling load calculated using the present FE model for the thinner cylindrical shell (geometry 2 and 3) is compared only with the numerically calculated load in the reference study, because no experiment was performed for the thinner shell.

Figure 5 shows the axially applied force vs. the deflection of the loaded end in the axial direction (end shortening) for the relatively thick shell (geometry 1) obtained by the present FE element model and the FE model developed in the reference study [23]. The numerically obtained curves are almost identical. The differences between the curves may be attributed to the differences in the mesh densities. Figure 5 also shows the equivalent stress contour plots of the present study as well as the pictures from the experiments corresponding to three load levels (*A*, *B*, *C*) after the onset of buckling. For the relatively thick shell, the yield load, N_y, is 30.79 kN, which is obtained by multiplying the yield strength with the cross-sectional area (πDt). The ratio of the critical buckling load, p_{cr}, to the yield load, N_y, was experimentally determined as 0.95 [23]. The value for this ratio (p_{cr}/N_y) predicted by the present nonlinear FE model is 0.94, which is very close to the experimental result.

For the thinner cylindrical shells, both linear and nonlinear buckling analyses are performed for geometry 2 and geometry 3 with L/D ratio being equal to 2 and 5, respectively. The numerical results of the present study together with that of the reference study are tabulated in Table 3. The numerical results compare well with that of the reference study. The critical buckling load predicted by the nonlinear analysis is about two times larger than that of the linear eigenvalue buckling analysis.

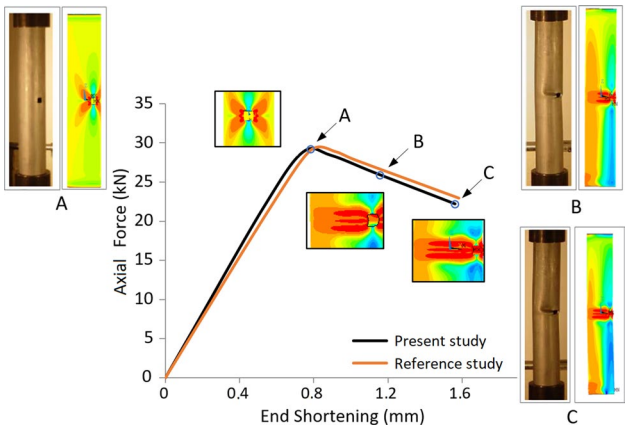

Fig. 5 Comparison of the experimental and numerical results of the reference study [23] and the numerical results of the present study for the relatively thick shell (geometry 1). **A**, **B**, and **C** are the pictures from the experiment [23] and the contour plots of the equivalent stress corresponding to three load levels after the onset of buckling

Table 3 Buckling loads (p_{cr}) numerically evaluated by the present and reference studies [23] for the thinner shells ($D/t = 450$)

	Buckling load, p_{cr} (N)	
	for $L = 2D$ (Geometry 2)	for $L = 5D$ (Geometry 3)
Linear analysis (present study)	328.2	293.1
Linear analysis [23]	333.4	296.9
Nonlinear analysis (present study)	734.7	638.9
Nonlinear analysis [23]	740.1	642.2

4 Optimization and results

4.1 The reference cylindrical shell for the optimization study

The geometry of the relatively thick cylinder (Geometry 1 in Table 1) is adopted except that the number of cutouts is two instead of one and the cutout size is increased from 7.5 mm×7.5 mm to 10 mm×10 mm. In this way, the cylinder bears more similarity to an aircraft exhaust case.

The nonlinear analysis of the reference geometry yields 22.05 kN for the critical buckling load. Linear eigenvalue analyses of the reference cylinder are carried out using OptiStruct and ANSYS. The critical buckling loads are obtained to be 76.63 kN and 76.83 kN, respectively. In the optimization study, the buckling load of the cylinder is maximized without increase in its mass by optimally designing the stiffeners introduced on its lateral surface. The mass of the unstiffened reference geometry is 22.3 g.

4.2 First level of optimization—topology optimization

In the topology optimization, stiffeners are introduced on the surface of the cylinder. The stiffener geometry is defined by its height, h, width, w, and orientation angle of its lateral surface, ϕ, as shown in Fig. 6. ϕ is taken as zero, and accordingly, the stiffeners are perpendicular to the cylinder surface.

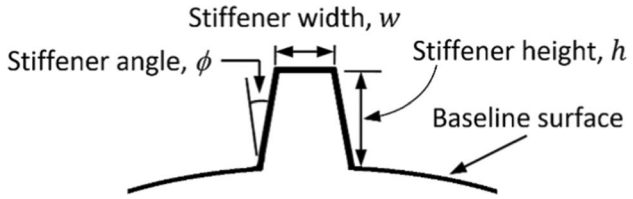

Fig. 6 Reference geometry for optimization

The height, h, is measured in the radial direction. h and w are the design variables defining the stiffener size and they are allowed to vary during the optimization. The design domain is the entire outer surface of the structure except small strips of one element size at the top and bottom as well as around the cutouts. No stiffener is generated in these regions. The thickness of the cylindrical shell remains constant during the first level of optimization.

The objective function, f, to be maximized is the critical bucking load, p_{cr}. The optimization problem can be expressed as

$$\begin{aligned} &\text{Maximize } f = p_{cr} \\ &\text{Subject to}: 0 \le h \le h_{\max} \\ &w_{\min} \le w \\ &0 \le V_{St} \le 0.4 V_{Sh} \end{aligned} \tag{3}$$

Constraints are imposed on the design variables, otherwise inappropriate values may be assigned to the design variables during optimization. For example, negative values may be assigned for dimensions or a very large value may be given for stiffener height, h, that is beyond the limit for which the shell theory is applicable. Other than these, the upper limit for h ($h_{\max}$) is not important in the topology optimization, because only optimal stiffener topology is obtained in the first level; stiffener sizes are optimized in the second level. Topology optimization is repeated for three different values of the upper limit for h, 0.5 mm, 1.0 mm, and 2.0 mm and similar stiffener configurations are obtained. The upper limit is then chosen as 1.0 mm. A lower limit should be selected for stiffener width, w. The width cannot be lower than the mesh size, which is 0.5 mm. In order to choose a suitable value, the optimization process is repeated using different lower limits on w ($w_{\min}$). Similar optimum stiffener configurations are obtained for the values of 0.625 mm, 1.0 mm 2.0 mm. In view of that, 1.0 mm is chosen for the minimum width constraint. If no upper limit were imposed to the volume of stiffeners, V_{St}, that the algorithm might place on the shell surface, the algorithm would generate stiffeners on the entire cylinder surface and set the stiffener height equal to its upper bound, which is 1.0 mm, to maximize the buckling strength. In order to prevent the algorithm from increasing the thickness uniformly, an upper limit is set for the maximum volume of stiffeners that can be generated on the shell surface. In this study, the upper limit for the volume fraction of stiffeners is chosen to be 0.4. Thus, the volume of the stiffeners,V_{St}, does not exceed 40% of the unstiffened shell volume, V_{Sh}, as described by Eq. (3). The lower limit is taken as zero.

By imposing the constraints expressed in Eq. (3), topology optimization is conducted for the reference shell geometry to obtain the optimum stiffener configuration on the shell surface for maximum buckling load capacity. Optimization is performed in OptiStruct, which evaluates the bucking resistance capacity based on a linear analysis. OptiStruct can use several alternative optimization algorithms such as the optimality criteria method, the convex approximation method, and the method of feasible directions. Optimality criteria method is selected for the present problem. Figure 7 shows the contour plot of the stiffener height, h, in the optimum stiffener configuration. The regions with red color indicate stiffeners having height close to its upper limit, 1.0 mm. They are the most critical regions, where local buckling may occur. The critical regions are the sides of the cutouts and the top and bottom ends, which are called "elephant-foot location" in the literature. In order to better see the stiffener pattern, contour plots of the stiffener height, h, are depicted for different ranges in Fig. 8. The algorithm positions stiffeners having a height close to 1.0 mm in regions that are in critical need of reinforcement against local buckling (Fig. 8a). The front and rear faces of the cylinder containing the openings are reinforced with stiffeners having a height

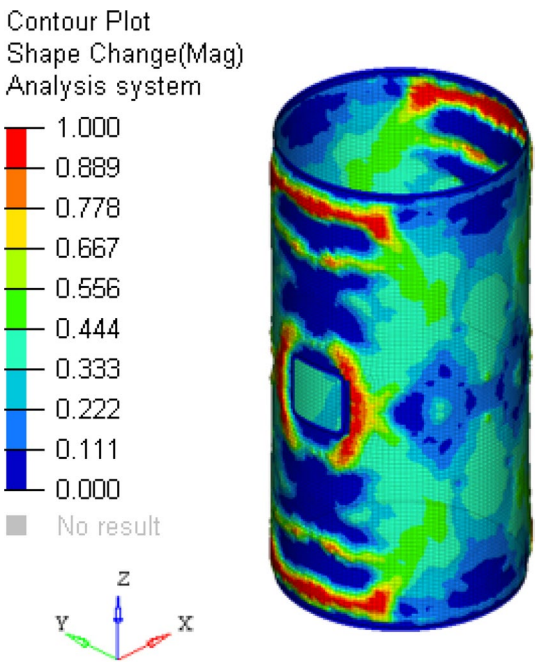

Fig. 7 Contour plot of the stiffener height, h, in the optimum stiffener configuration

larger than 0.6 mm. On the sides of the cylinder, on the other hand, the stiffener height is less than 0.6 mm.

4.3 Second level of optimization—stiffener height optimization

4.3.1 Stiffener pattern

Different stiffener patterns can be distinguished in different regions of the shell surface from the contour plots of the topology optimization as shown in Figs. 8 and 9. The orange-colored stiffener corresponds to 0.6–1.0 mm range of thickness in the contour plot given in Fig. 8a. They provide the main support around the cutouts and the elephant-foot locations in the structure. The widths of the stiffeners are directly obtained from the topology optimization results; accordingly, the cutout and elephant-foot locations have 2-mm-width stiffeners, the width of the others is 1 mm. Although no connection is observed between the stiffeners around the cutouts and the stiffeners at the elephant-foot locations in 0.6–1.0-mm-height plot (Fig. 8a), they are connected with the first type of stiffeners for a better transmission of load and also considering that they are connected with stiffeners in the 0.3–0.6-mm-height range. The topology optimization algorithm creates a large region in the 0.3–0.6-mm-height range. For those regions, rather than thickening the entire area, grid-stiffeners are generated with orthogrid pattern having 0.3 mm width to avoid weight increase for locations where a large area needs to be thickened according to the results shown in Fig. 8b. The regions that the algorithm generated stiffeners with less than 0.3 mm height are left unstiffened in the second-level optimization. As the third type of stiffeners, the blue-colored stiffeners with 1.0 mm width are used as dividers of those regions.

The reason that the configuration found by OptiStruct is not directly used in the second level is that the pattern is too complex to define with a feasible number of design variables.

4.3.2 Objective function, design variables, and constraints

The objective of the optimization is to maximize the critical buckling load of the structure. Because the optimization problems are posed as minimization problems in the

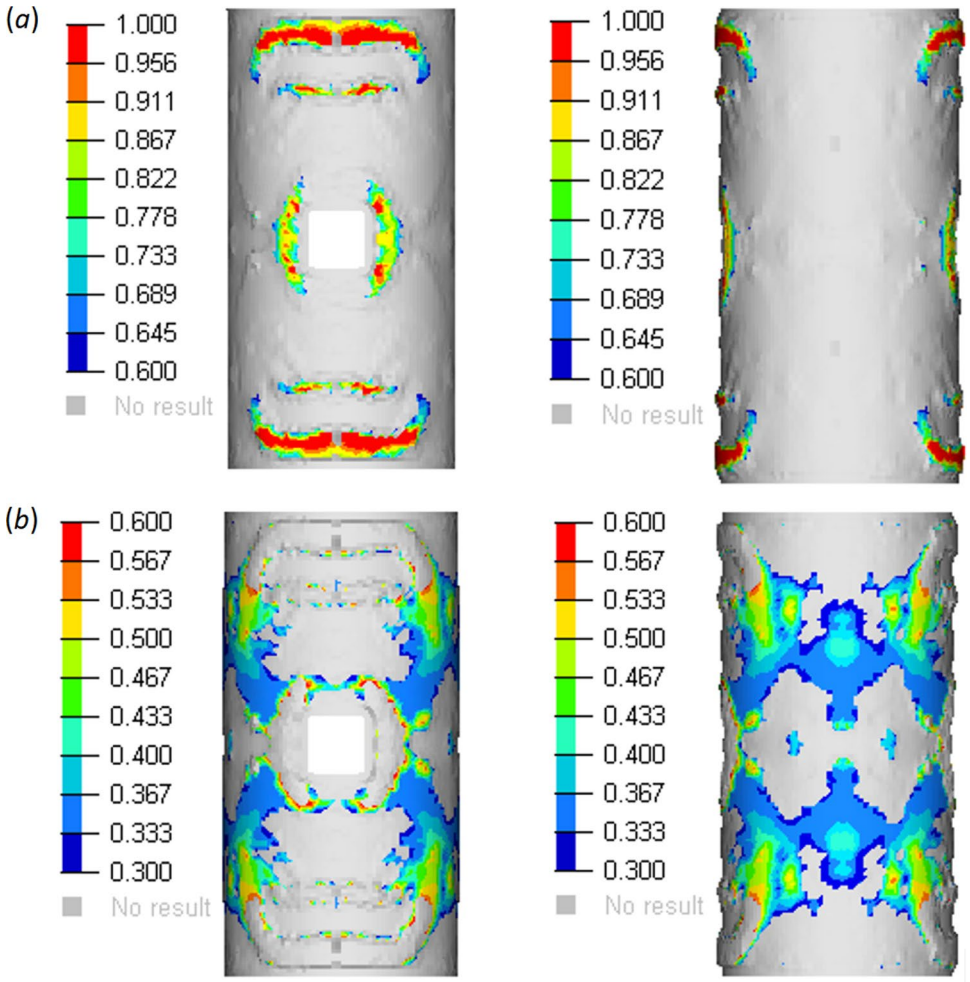

Fig. 8 Contour plots for different ranges of height, *h*, in mm **a** 0.6–1.0, **b** 0.3–0.6

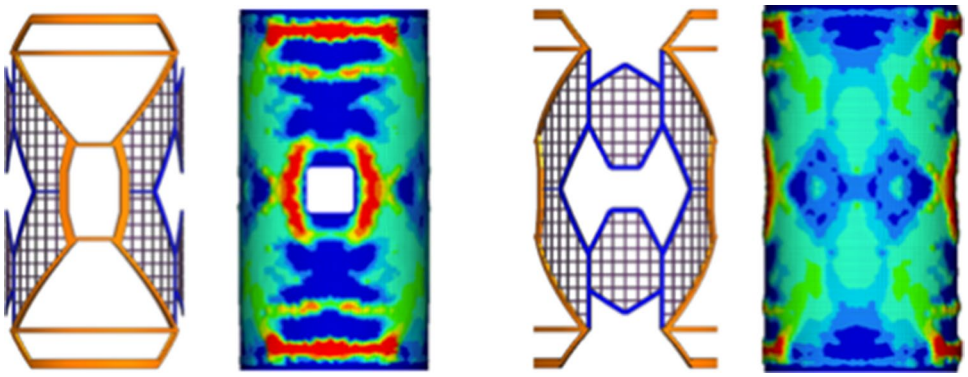

Fig. 9 Front and side views of the stiffeners in the CAD model and the topology optimization result

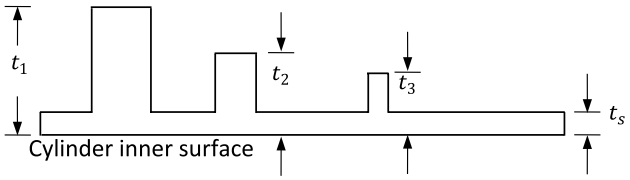

Fig. 10 Schematic representation of the thicknesses at stiffener locations, t_i, as they are defined in the optimization code and the shell thickness, t_s

standard implementation of the search algorithm, the objective function is taken as negative of the buckling load. This is mathematically equivalent to the problem of maximizing the buckling resistance of the structure.

In the second level, the cylinder shell thickness, t_s, and the thicknesses at the stiffener locations, t_i, shown in Fig. 9 are taken as the optimization variables as opposed to the first-level optimization, where the cylinder shell thickness is taken constant and the heights of the stiffeners, h_i, and their positions are varied. The stiffener thicknesses, t_i, include stiffener height, h_i, as well as the cylinder shell thickness, t_s as $t_i = h_i + t_s$ as shown in Fig. 10. The widths of the stiffeners are kept constant. Because the total weight of the cylinder is constrained to be constant, the variables are not independent. The cylinder shell thickness is considered as the dependent variable. As the thicknesses at stiffener locations are changed by the algorithm in each iteration, the cylinder shell thickness is recalculated to keep the weight the same as the unstiffened cylinder.

No design constraints are defined for the design variables in terms of upper or lower bounds besides the mass constraint for the stiffened cylinder. Since the stiffener configuration is not changed in the second level of optimization, the surface area of each group of stiffener remains the same while the thicknesses are varied. Whenever a new configuration is generated by Nelder–Mead algorithm, surface areas of the stiffeners are multiplied by the corresponding thickness to obtain the volume of the stiffeners. This is then subtracted from the total volume of the unstiffened geometry. The resulting value is divided by the unstiffened shell surface area to find the cylinder shell thickness. That means the mass constraint is imposed by eliminating the dependent variable.

4.3.3 FE modeling

In order to evaluate the value of the objective function, nonlinear bucking analyses are conducted using ANSYS solver. A Python code is developed to implement the optimization algorithm and perform the structural analyses.

The structure is modeled using Shell-181 type of element in ANSYS. The stiffeners are integral parts of the cylindrical shell as opposed to some models that define bounded contact between the cylinder shell and the stiffeners. Thickness at a stiffener location is defined as shell thickness; this means that the thickness of a finite element, t_i, is the sum of the cylinder shell thickness, t_s, and the stiffener height at its location, h_i. The stiffener material is defined the same as that of the shell. 0.3 mm mesh size is used for thin stiffeners and 0.5 mm is used for the rest. The meshed stiffened geometry in ANSYS is shown in Fig. 11.

4.3.4 Second-level optimization results

Local search optimization is performed via Nelder–Mead method. Initial values of the design variables are arbitrarily chosen as 2.00 mm, 1.50 mm, and 1.50 mm. These are the thicknesses at the locations of the first, second, and third type of stiffeners described in Sects. 4.3.1 and 4.3.2. Nelder–Mead algorithm requires $n+1$ number of starting points. The other starting points are defined by reducing 10% from the initial value of one of the design variables and keeping the rest of them the same. Repeating this process for other variables, three more starting points are obtained. Convergence criterion for Nelder–Mead algorithm is defined as %1, which means the optimization process stops either when the differences in the values of the design variables or the objective function are less than %1 for the best and the worst configurations. The iteration values of the design

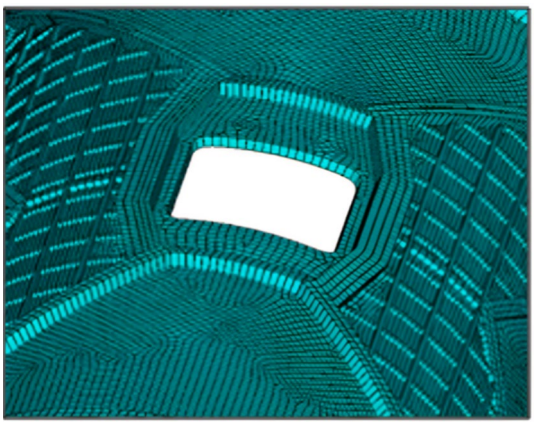

Fig. 11 The meshed model of the stiffened cylindrical shell in ANSYS

variables in terms of stiffener thickness and the corresponding shell thickness are given in Fig. 12. The results show that the first type of stiffener, which provides support around the cutouts and the elephant-foot locations, is the only group of stiffeners that should exist on the shell surface for maximum buckling strength. As indicated in Fig. 10, the thickness at a stiffener location also includes the cylinder shell thickness. It can be observed from Fig. 12 that the converged values of t_2 and t_3 are very close to the cylinder shell thickness, t_s, which means they actually do not make a significant contribution on the buckling strength of the structure as opposed to the first type of stiffener. The search algorithm increases t_1 and t_s at the expense of t_2 and t_3 to increase the buckling load; thus, those two stiffener groups located on the lateral surface of the cylinder should be eliminated from the final stiffener configuration. Figure 13 shows the iteration values of the critical buckling load versus the number of iterations. The results show that sometimes stiffener thickness takes a value lower than the shell thickness, t_s, which introduces another geometrical imperfection causing considerable decrease in the buckling load-carrying capacity of the structure. The optimum value of the cylinder shell thickness, t_s, is 0.734 mm, and the optimum thickness of the first stiffener, t_1, is 2.194 mm; this means its height, h_1, is 1.460 mm. Because the difference between the cylinder shell thickness, t_s, and the converged thickness values of other two groups of stiffeners, t_2 and t_3, is very small, their height is neglected. The critical buckling load of the optimum stiffened cylinder is 26.89 kN, which indicates 22% increase compared to 22.05 kN buckling strength of the reference unstiffened cylindrical shell. The optimization process is repeated a number of times starting from different initial values of the design variables and the same result is obtained.

Figure 14 shows the buckled shapes of the optimum stiffened geometry and the unstiffened geometry. In both geometries, buckling first occurs in the section containing the holes. However, the stiffeners delay buckling as shown in Fig. 15, where the load versus end-shortening graphs are presented. As seen in Fig. 15, post-buckling strength of the optimum stiffened geometry is significantly higher than that of the unstiffened reference shell.

5 Conclusions

In this study, the buckling load capacities of stiffened and unstiffened cylindrical shells with cutouts are numerically investigated using ANSYS software. The FE model for an unstiffened cylindrical shell with a cutout is validated by comparing its predictions with the results reported by Han et al. [23]. Topology optimization is performed to find the optimum stiffener pattern over the shell surface that maximizes the buckling strength using OptiStruct software. The optimization process produces a non-uniform stiffener pattern over the shell surface; large stiffeners around the cutouts and near the top and bottom edges, but smaller sized stiffeners away from these regions. After optimizing the stiffener pattern, the heights of the stiffeners and the shell thickness are optimized using Nelder–Mead search algorithm.

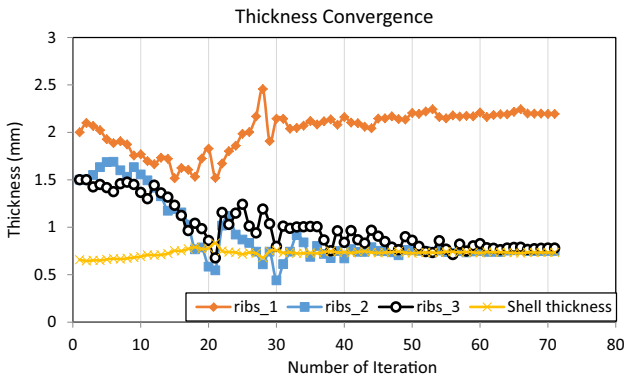

Fig. 12 Iteration values of the design variables and the shell thickness

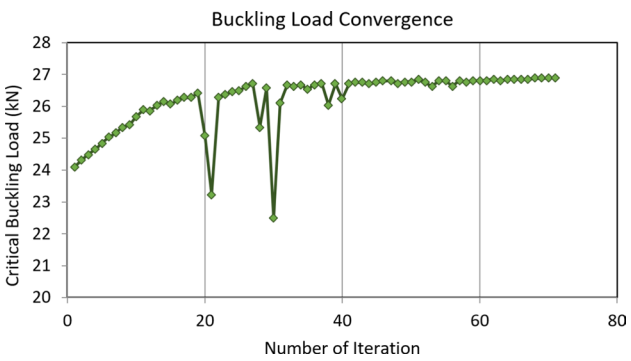

Fig. 13 Iteration values of the objective function (the critical buckling load)

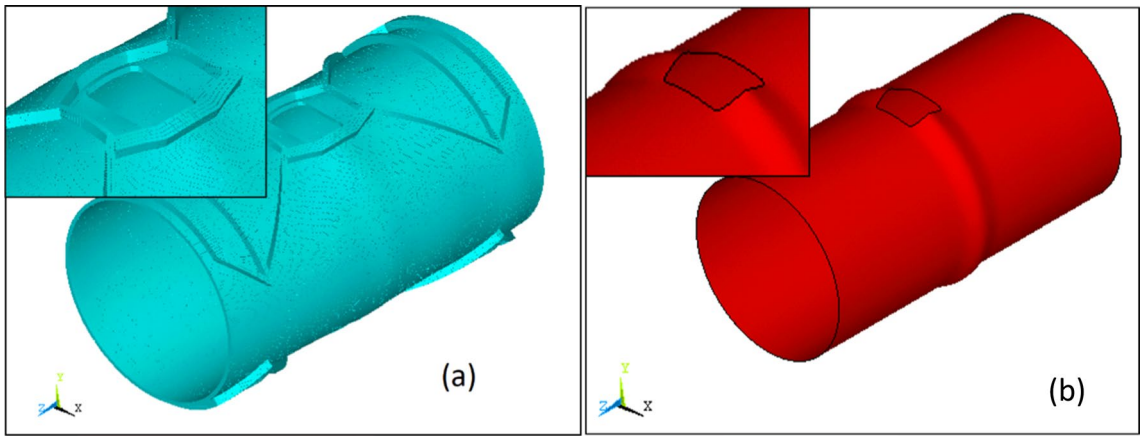

Fig. 14 Buckled shapes of **a** the optimum stiffened geometry and **b** the unstiffened geometry

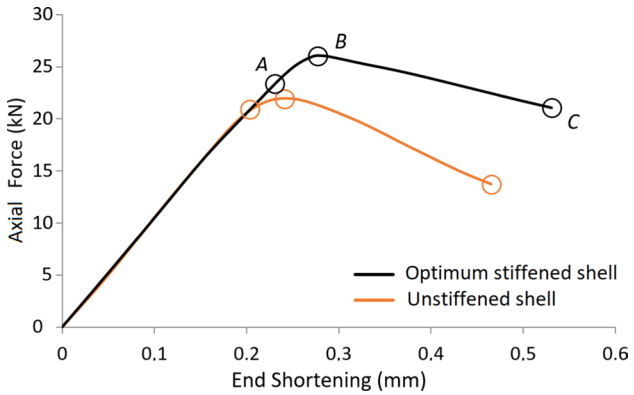

Fig. 15 Force versus end-shortening curves for the optimum stiffened and unstiffened geometries having the same weight

The results indicate that the stiffeners are most effective in recovering the structural strength weakened due to the geometrical imperfection, when they are placed at the sides of the cutouts and near the top and bottom edges. As opposed to the first-level optimization results, where stiffeners are generated almost all over the shell surface, in the second-level optimization, no stiffeners are generated on surfaces away from the cutouts and the edges. This difference may be attributed to the difference in the optimization methods in different levels and also to the use of linear buckling analysis in the first level and nonlinear analysis in the second. The nonlinear analysis result is more reliable considering the correlation with the experimental results. The critical buckling load of the optimum stiffened shell is 22% higher compared to the unstiffened shell having the same mass. Besides, post-buckling strength is significantly higher.

Funding No funding was received for conducting this study.

Declarations

Conflict of interest There are no conflicts of interest with other people or organizations.

References

1. Weller T, Singer J (1977) Experimental studies on the buckling under axial compression of integrally stringer-stiffened circular cylindrical shells. J Appl Mech Trans ASME 44(4):721–730. https://doi.org/10.1115/1.3424163
2. Hotała E, Skotny Ł (2014) Experimental investigations on the stability of stiffened cylindrical shells of steel silos. J Constr Steel Res 96:81–94. https://doi.org/10.1016/j.jcsr.2014.01.009
3. Hui-shen S, Pin Z, Tie-yun C (1991) Buckling and postbuckling of stiffened cylindrical shells under axial compression. Appl Math Mech 12(12):1195–1207. https://doi.org/10.1007/BF02456059
4. Hu Y, Baniotopoulos C, Yang J (2014) Effect of internal stiffening rings and wall thickness on the structural response of steel wind turbine towers. Eng Struct 81:148–161
5. Zhu Y, Dong JH, Gao BJ (2015) Buckling analysis of thin walled cylinder with combination of large and small stiffening rings under external pressure. Procedia Eng 130:364–373. https://doi.org/10.1016/j.proeng.2015.12.229
6. Yang Y, Li J-J, Zhang Y, He Q, Dai H-L (2021) A semi-analytical analysis of strength and critical buckling behavior of underwater ring-stiffened cylindrical shells. Eng Struct 227:111396. https://doi.org/10.1016/j.engstruct.2020.111396
7. Foryś P (2015) Optimization of cylindrical shells stiffened by rings under external pressure including their post-buckling behaviour. Thin-Walled Struct 95:231–243. https://doi.org/10.1016/j.tws.2015.07.012
8. Bagheri M, Jafari AA, Sadeghifar M (2011) A genetic algorithm optimization of ring-stiffened cylindrical shells for axial and radial buckling loads. Arch Appl Mech 81(11):1639–1649. https://doi.org/10.1007/s00419-011-0507-2
9. Sadeghifar M, Bagheri M, Jafari AA (2010) Multiobjective optimization of orthogonally stiffened cylindrical shells for minimum weight and maximum axial buckling load. Thin-Walled Struct 48(12):979–988. https://doi.org/10.1016/j.tws.2010.07.006
10. Wang B, Hao P, Li G, Tian K, Du K, Wang X, Zhang X, Tang X (2014) Two-stage size-layout optimization of axially compressed

stiffened panels. Struct Multidiscip Optim 50(2):313–327. https://doi.org/10.1007/s00158-014-1046-6
11. Wang B, Tian K, Zhou C, Hao P, Zheng Y, Ma Y, Wang J (2017) Grid-pattern optimization framework of novel hierarchical stiffened shells allowing for imperfection sensitivity. Aerosp Sci Technol 62:114–121. https://doi.org/10.1016/j.ast.2016.12.002
12. Uys PE, Farkas J, Jármai K, van Tonder F (2007) Optimisation of a steel tower for a wind turbine structure. Eng Struct 29(7):1337–1342
13. Zhao Y, Chen M, Yang F, Zhang L, Fang D (2017) Optimal design of hierarchical grid-stiffened cylindrical shell structures based on linear buckling and nonlinear collapse analyses. Thin-Walled Struct 119:315–323. https://doi.org/10.1016/j.tws.2017.06.019
14. Tian K, Wang B, Zhang K, Zhang J, Hao P, Wu Y (2018) Tailoring the optimal load-carrying efficiency of hierarchical stiffened shells by competitive sampling. Thin-Walled Struct 133:216–225. https://doi.org/10.1016/j.tws.2018.03.029
15. Meng Z, Luo X, Zhou H (2022) Lightweight design of arcuately stiffened cylindrical shells based on smeared stiffener method and active learning strategy. Thin-Walled Struct 174:109167. https://doi.org/10.1016/j.tws.2022.109167
16. Meng Z, Hao P, Li G, Wang B, Zhang K (2015) Non-probabilistic reliability-based design optimization of stiffened shells under buckling constraint. Thin-Walled Struct 94:325–333. https://doi.org/10.1016/j.tws.2015.04.031
17. Hao P, Wang B, Tian K, Li G, Sun Y, Zhou C (2017) Fast procedure for non-uniform optimum design of stiffened shells under buckling constraint. Struct Multidiscip Optim 55(4):1503–1516. https://doi.org/10.1007/s00158-016-1590-3
18. Ghazijahani TG, Jiao H, Holloway D (2015) Structural behavior of shells with different cutouts under compression: an experimental study. J Constr Steel Res 105:129–137. https://doi.org/10.1016/j.jcsr.2014.10.020
19. Alsalah A, Holloway D, Ghazijahani TG (2017) Recovery of capacity lost due to openings in cylindrical shells under compression. J Constr Steel Res 137:169–179. https://doi.org/10.1016/j.jcsr.2017.06.006
20. Hao P, Wang B, Tian K, Li G, Du K, Luan Y (2016) Integrated optimization of hybrid-stiffness stiffened shells based on sub-panel elements. Thin-Walled Struct 103:171–182. https://doi.org/10.1016/j.tws.2016.01.027
21. Hao P, Wang B, Tian K, Liu H, Wang Y, Niu F, Zeng D (2017) Simultaneous buckling design of stiffened shells with multiple cutouts. Eng Optim 49(7):1116–1132. https://doi.org/10.1080/0305215X.2016.1235328
22. Jullien JF, Limam A (1998) Effects of openings of the buckling of cylindrical shells subjected to axial compression. Thin-Walled Struct 31(1–3):187–202
23. Han H, Cheng J, Taheri F, Pegg N (2006) Numerical and experimental investigations of the response of aluminum cylinders with a cutout subject to axial compression. Thin-Walled Struct 44(2):254–270. https://doi.org/10.1016/j.tws.2005.11.003
24. Starnes JH Jr (1972) Effect of a circular hole on the buckling of cylindrical shells loaded by axial compression. AIAA J 10(11):1466–1472. https://doi.org/10.2514/3.6644
25. Tian K, Li H, Huang L, Huang H, Zhao H, Wang B (2020) Data-driven modelling and optimization of stiffeners on undevelopable curved surfaces. Struct Multidiscip Optim 62(6):3249–3269. https://doi.org/10.1007/s00158-020-02675-4
26. Li H, Li Z, Cheng Z, Zhou Z, Wang G, Wang B, Tian K (2022) A data-driven modelling and optimization framework for variable-thickness integrally stiffened shells. Aerosp Sci Technol 129:107839. https://doi.org/10.1016/j.ast.2022.107839
27. ANSYS (2017) 16.0 User's Manual, 2017
28. Mallon NJ, Fey RHB, Nijmeijer H (2010) Dynamic stability of a base-excited thin orthotropic cylindrical shell with top mass: Simulations and experiments. J Sound Vib 329(15):3149–3170. https://doi.org/10.1016/j.jsv.2010.02.007